Robotica (2005) volume 23, pp. 457–465. © 2005 Cambridge University Press
doi:10.1017/S0263574704001535 Printed in the United Kingdom

An Experimental Optical Three-axis Tactile Sensor for Micro-Robots

Masahiro Ohka*, Yasunaga Mitsuya**, Isamu Higashioka*** and Hisanori Kabeshita†

(Received in Final Form: November 22, 2004)

SUMMARY

This paper describes a micro-optical three-axis tactile sensor capable of sensing not only normal force, but also shearing force. The normal force was detected from the integrated gray-scale values of bright pixels emitted from the contact area of conical feelers. The conical feelers were formed on a rubber sheet surface that maintains contact with an optical waveguide plate. The shearing force was detected from horizontal displacement of the conical feeler. In the experiments, a precise multi-axial loading machine was developed to measure sensing characteristics of the present sensor. Results show that the normal force was specified uniquely under combined force conditions and that the shearing force was specified by modifying the relationship between the shearing force and the horizontal displacement on the basis of normal force. We formulated a set of expressions to derive the normal force and the shearing force by taking into account this modification. Furthermore, calibration coefficients were identified for transforming the integration of gray-scale values into the normal force and for transforming the horizontal displacement into the shearing force. This result suggests that the expressions can estimate the normal force and the shearing force in wide-load regions.

KEYWORDS: Tactile sensor; Optical measurement; Three-axis; MEMS; Micro-robot.

I. INTRODUCTION

Tactile sensors have been developed using measurements of strain produced in sensing materials that are detected using physical quantities such as electric resistance and capacity, magnetic intensity, voltage and light intensity.[1] The optical tactile sensor, which is one of these sensors, comprises an optical waveguide plate, which is made of transparent acrylic and is illuminated along its edge by a light source.[2–5] The light directed into the plate remains within it due to the total internal reflection generated, since the plate is surrounded by air having a lower refractive index than the plate. A rubber sheet featuring an array of conical feelers is placed on the plate to keep the array surface in contact with the plate. If an object contacts the back of the rubber sheet, resulting in contact pressure, the feelers collapse, and at the points where these feelers collapse, light is diffusely reflected out of the reverse surface of the plate because the rubber has a higher refractive index than the plate. The distribution of contact pressure is calculated from the bright areas viewed from the reverse surface of the plate.

The sensitivity of the optical tactile sensor can be adjusted by texture morphology and hardness of the sheet. The texture can be easily made fine with a mold suited for micro-machining because the texture is controlled by adjusting the process of pouring the rubber into the mold. This process enables the production of a micro-tactile sensor with high density and sensitivity by using the abovementioned principle of the optical tactile sensor. However, this method can detect only distributed pressure applied vertically to the sensing surface and needs a new idea to sense the shearing force. In this paper, the original optical tactile sensor is called a uni-axial optical tactile sensor.

A micro-robot;[6–8] would inspect and remedy problems on the inside of blood vessels, digestive organs, or small pipes in machines. When inspecting and maintaining these vessels, the robot would inevitably contact their walls. The robot would also be programmed to discover affected or defective parts, such as tumors or cracks formed in vascular walls. For such a micro-machine to work as described above, a sensitive tactile would be vital to make the machine effective. In addition, the machine would be required to remove any object attached to the inside a blood-vessel or pipe wall. It therefore becomes necessary to measure not only the normal force but also the shearing force. Accordingly, a tactile sensor for mounting on a micro-machine should be capable of detecting three-axis force.

If we produce molds with complex structures to make rubber sheets comprising two types of feeler arrays attached to opposite sides of the rubber sheet, it will be possible to improve the uni-axial tactile sensor for use in three-axis tactile sensors.[9–11] One of these types is a sparse array of columnar feelers that make contact with the object to be recognized; the other is a dense array of conical feelers that maintain contact with the waveguide plate. Because each columnar feeler is arranged on 2-by-2 conical feelers so that it presses against four conical feelers under the action of an applied force, three components of the force vector are identified by the four contact areas of the conical feelers.

* Corresponding author: Department of Complex Systems Science, Graduate School of Information Science, Nagoya University, Furo-cho, Chikusa-ku, Nagoya, 464-8601 (Japan). E-mail: ohka@is.nagoya-u.ac.jp
** Dept. of Micro System Engng, Graduate School of Engng, Nagoya University.
*** Mitsubishi Electric, Co. (Japan).
† Hitachi RE System Co. LTD. (Japan).

However, the three-axis tactile sensor is too complicated to be miniaturized, thus a simple structure is required to simplify processing and assembly for the sensor.

In an effort to solve the above problem, this study is aimed at developing a three-axis tactile sensor for mounting on a microscope-shaped micro-robot. For ease of micro-miniaturization, the sensor is structured as simply as possible, with its three-axis force rendered measurable by the effective application of an algorithm. We have previously introduced a principle for a new three-axis tactile sensor using the optical uni-axial tactile sensor as the sensor hardware and image data processing techniques to detect three-axis force. The principle was validated using a large, experimental tactile sensor.[12]

In the algorithm, an array of conical feelers is adopted as the texture of the rubber sheet. If combined normal and shearing forces are applied to the sensing surface, the conical feelers make contact with the acrylic board and are subjected to compressive and shearing deformation. The gray-scale value of the image of contact area is distributed as a bell shape, and since it is proportional to pressure caused on the contact area, it is integrated over the contact area to calculate the normal force. Lateral strain in the rubber sheet is caused by the horizontal component of the applied force and it makes the contact area with the conical feelers move horizontally. The horizontal displacement of the contact area is proportional to the horizontal component of the applied force, and is calculated as a centroid of the gray-scale value. Since the horizontal movement of the centroid has two degrees of freedom, both horizontal movement and contact area are used to detect the three components of the applied force.

In the present paper, we perform a series of FEM contact simulations that take into account contact friction to precisely examine the principle of three-axis force detection. Next, we outline the development of an experimental micro-tactile sensor comprising an acrylic board, a microscope, a CCD camera and a silicon rubber sheet having a 10-by-12 array of conical feelers of which the bottom radius and height are 150 and 100 μm, respectively. The combined force-testing machine is developed to apply small combined forces to the micro-tactile sensor. Using this testing device, we perform validation experiments and obtain calibration data for the tactile sensor.

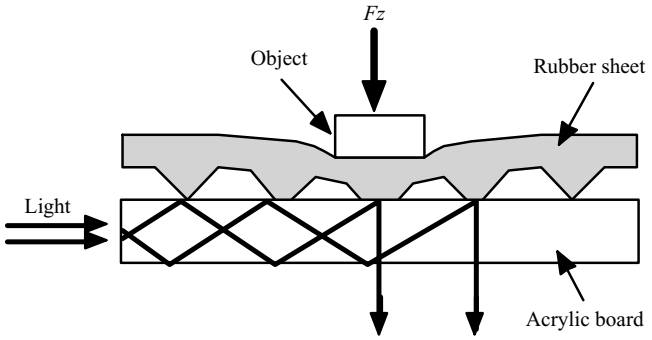

Fig. 1. Principle of an optical uni-axis tactile sensor.

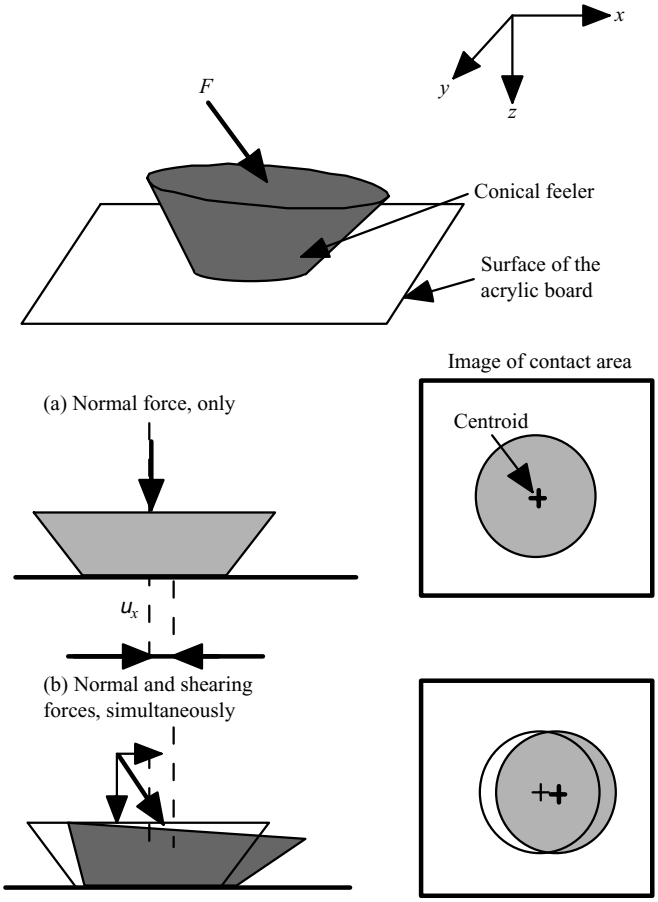

Fig. 2. Principle of an optical three-axis tactile sensor.

II. PRINCIPLE

II.1. Optical uni-axial tactile sensor

As Figure 1 shows, the optical uni-axial tactile sensor consists of a rubber sheet, an acrylic board, a CCD camera, and a light source. Beams of light, emitted from the light source to the edge of the acrylic board, are totally enclosed and reflected inside the acrylic board. When an object adheres to the back side of the rubber sheet and compresses the conical feelers, the contact areas of the conical feelers cause the light to scatter, and are observed from the rear side of the acrylic board. The distribution of the normal force working on the rubber can be measured in terms of light intensity distribution caused by the contact areas.

II.2. Optical three-axis tactile sensor for micro-robots

The three-axis force detection principle of the present sensor is shown in Figure 2. To provide a definition for the force direction, a Cartesian coordinate frame is added to the figure. If the base of the conical feeler accepts three-axis force, it contacts the acrylic board, which accepts both compressive and shearing deformation. Because the light scatters on the contact area, the gray-scale value of the contact image acquired by the CCD camera distributes as a bell shape, in which the gray-scale intensity is highest at the centroid and decreases with increasing distance from the centroid.

In the following section it is found that the gray-scale $g(x, y)$ of the contact image is proportional to the contact

https://doi.org/10.1017/S0263574704001535 Published online by Cambridge University Press

pressure $p(x, y)$ caused by the contact between the conical feeler and the acrylic board, that is,

$$p(x, y) = Cg(x, y), \tag{1}$$

where C and $g(x, y)$ are the conversion factor and the gray-scale distribution, respectively.

If S is designated as the contact area of the acrylic board and the conical feeler, the vertical force, F_z is obtained by integrating the pressure over the contact area as follows:

$$F_z = \int_S p(x, y)dS. \tag{2}$$

If Eq. (1) is substituted for Eq. (2),

$$F_z = \int_S Cg(x, y)\, dS \equiv CG, \tag{3}$$

where the integration of $g(x, y)$ over the contact area is denoted as G.

Next, to formulate horizontal components of the force vector F_x and F_y, x- and y-coordinates of the centroid of gray-scale value, (X_G, Y_G) are calculated by

$$X_G = \frac{\int_S g(x, y)x\, dS}{\int_S g(x, y)\, dS}, \tag{4}$$

and

$$Y_G = \frac{\int_S g(x, y)y\, dS}{\int_S g(x, y)\, dS}. \tag{5}$$

In the integrations, the integration area S can be enlarged as long as it does not invade adjacent contact areas, because $g(x, y)$ occupies almost no space outside contact area. Since the shearing force induces axial strain in the silicon rubber sheet, the contact area of the conical feeler moves in the horizontal direction. The x- and y-components of the movement are denoted as u_x and u_y, respectively. They are variations in the abovementioned X_G and Y_G:

$$u_x = X_G^{(t)} - X_G^{(t-1)} \tag{6}$$

$$u_y = Y_G^{(t)} - Y_G^{(t-1)}, \tag{7}$$

where the superscripts (t) and $(t-1)$ represent current and prior steps, respectively.

If friction between the silicon rubber and the acrylic board is ignored, x- and y-directional forces, F_x and F_y are calculated as follows:

$$F_x = K_x u_x, \tag{8}$$

$$F_y = K_y u_y, \tag{9}$$

where K_x and K_y are x- and y-directional spring constants of the rubber sheet, respectively.

III. CONTACT ANALYSIS USING FEM

III.1. Conical feeler's contact deformation caused by normal force

Here we examine the relationship between the gray-scale value of the contact image and contact pressure on the contact area to validate the sensing principle for normal force. In the investigation FEM software (ABAQUS/Standard, Hibbitt, Karlsson & Sorensen, Inc.) was used and contact analysis between the conical feeler and the acrylic board was performed. To simulate the same condition as the experiments described in Sections 4 and 5, we measured the morphology of the mold for the silicon rubber sheet using a laser microscope (ILM21W, Laser Tech, Inc.). Figure 3(a) shows a mesh model of the conical feeler generated on the basis of the obtained morphologic data; actually, the conical feeler does not have a perfect conical shape, as shown in Figure 3(a). The radius and height of the conical feeler are 150 and 100 μm, respectively.

The Young's modulus of the silicon rubber sheet was presumed to be 0.476 MPa. The Poisson's ratio was assumed to be 0.499 because incompressibility of rubber, which is assumed in mechanical analysis for rubber, holds for the value of Poisson's ratio. Only one quarter of the conical feeler was analyzed because the conical feeler is assumed to be symmetric with respect to the z-axis. Normal displacements on cutting planes of XZ and YZ were constrained to satisfy the symmetrical deformation, and the acrylic board was modeled as a rigid element with full constraint.

The three-dimensional (3-D) model was used for a simulation in which a normal force was applied to the top surface of the conical feeler. The calculated result will be evaluated in a later section with the experimental results.

III.2. Mechanism of feeler's movement due to shearing force

In the previous explanation about the principle of shearing force detection, we derived Eqs. (8) and (9) while ignoring the friction between the conical feeler and the acrylic board. In this section, we analyze the conical feeler's movement while taking into account the friction to modify Eqs. (8) and (9). Figure 3(b) shows a 2-D model with which we examine the deformation mechanism and the conical feeler movement under the combined loading of normal and shearing forces.

In the 2-D model, the same height and radius values for the conical feeler are adopted as those of the previous 3-D model. The thickness of the rubber sheet is 300 μm and both sides of the rubber sheet are constrained. Young's modulus and Poisson's ratio are also adopted at the same values as those of the previous 3-D model. The acrylic board was modeled as a rigid element with full constraint as well. The coefficient of friction between the conical feeler and the acrylic board is assumed to be 1.0 because this is a common value for the coefficient of friction between rubber and metal. The critical shearing force, $\tau_{\max}$, which means the limitation value for no slippage occurring, is presumed to be 0.098 MPa.

Combined loadings of normal and shearing forces were applied to the upper surface of the rubber sheet. The conical feeler's movement, u_x, was calculated with Eq. (4) while maintaining the vertical component of line force f_z, a

https://doi.org/10.1017/S0263574704001535 Published online by Cambridge University Press

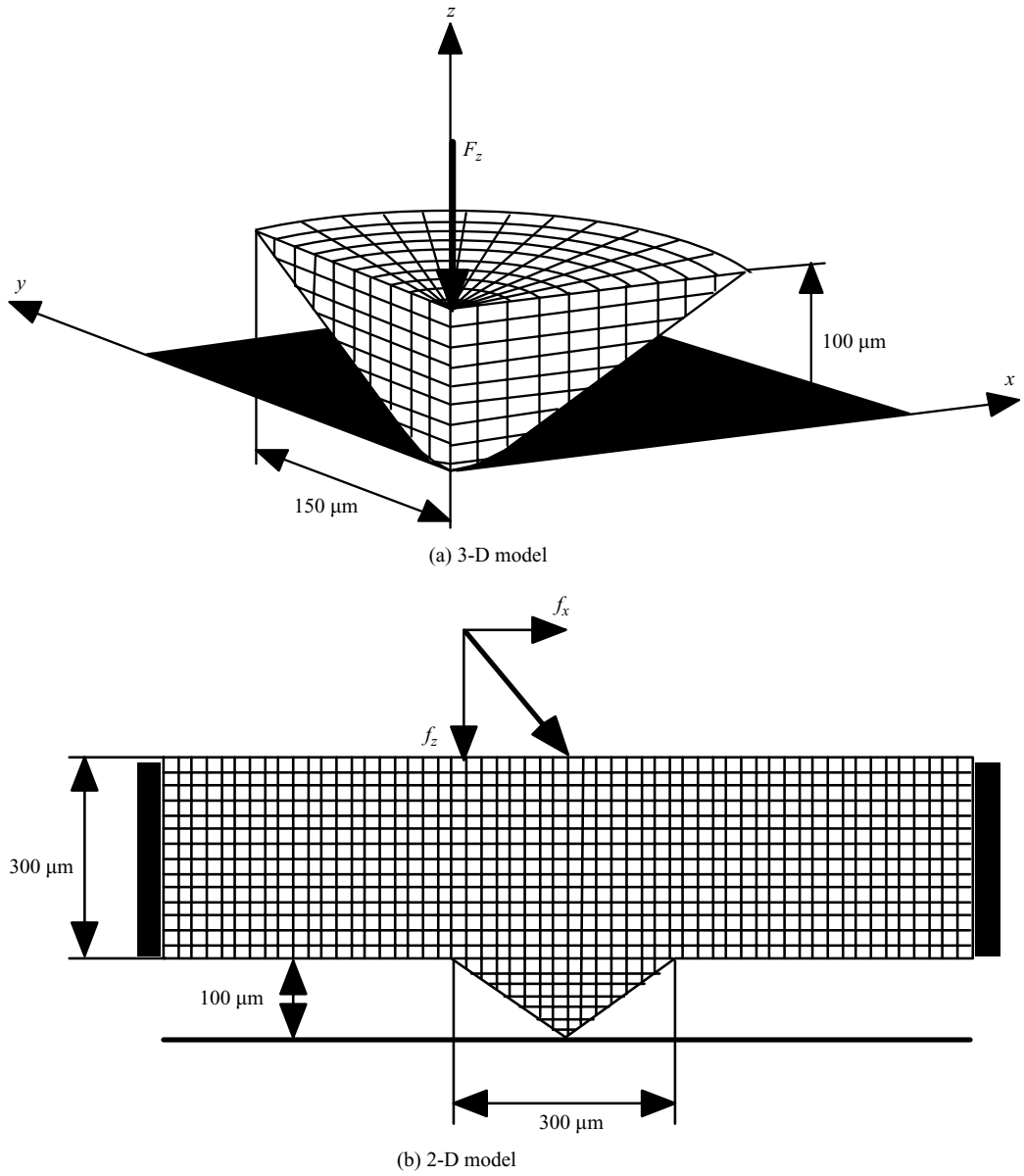

Fig. 3. Models for FEM analysis (a) 3-D model (b) 2-D model.

constant value, and increasing the horizontal component of line force f_x, where the components of line forces f_x and f_z are x- and z-directional force components per depth length, respectively. Since the conical feeler's movement is calculated as movement of the gray-scale's centroid in the later experiments, in this section it is calculated as the movement of the distributed pressure's centroid. We calculated five line force conditions, $f_z = 9.8$, 14.7, 19.6, 24.5 and 29.4 mN/mm, to examine the influence of vertical force on the movement of the centroid of the distributed pressure.

Figure 4 shows the relationships that exist between the movement of the centroid of the distributed pressure, u_x, and the horizontal component of the line force, f_x. As shown in that figure, there are bi-linear relationships where the inclination is small in the range of the low-horizontal line force and becomes large in the range of the high-horizontal line force, exceeding a threshold. This threshold depends on

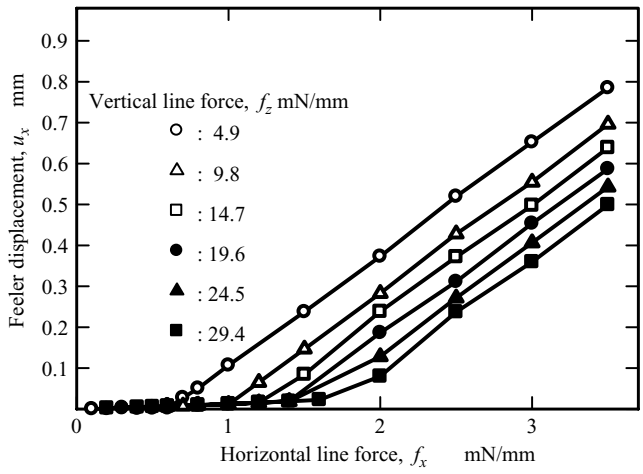

Fig. 4. Relationship between horizontal feeler movement and horizontal line force.

https://doi.org/10.1017/S0263574704001535 Published online by Cambridge University Press

the vertical line force and increases with increasing vertical line force, because the bi-linear relationship moves to the right with an increase in the vertical line force.

The abovementioned bi-linear relationship can be explained with the Coulomb friction law and elastic deformation of the conical feeler accepting both normal and shearing forces. That is, the conical feeler accepts shearing deformation while contacting the acrylic board when shearing stress arising between the acrylic board and conical feeler does not exceed a resolved shearing stress. At this stage of deformation, since the contact area changes from a circular to a pear shape, the centroid of distributed pressure moves in accordance with this change in contact shape. The inclination of the relationship between u_x and f_x is small in the range of a low loading level due to the tiny displacement occurring in the abovementioned deformation stage. In the subsequent stage, when the shearing stress exceeds the resolved shearing stress $\tau_{\max}$, then according to the increase of the lateral force, the friction state switches over from static to dynamic and the conical feeler moves markedly due to slippage occurring between the conical feeler and the acrylic board. The inclination of $u_x - f_x$, therefore, increases more in the range of a high shearing force level than in the range of a low shearing force.

Taking into account the abovementioned deformation mechanism, we attempt to modify Eqs. (8) and (9). First, we express the displacement of centroid movement at the beginning of slippage as u_{x1}. If $u_x = u_{x1}$ is adopted as the threshold, the relationship between u_x and F_x is expressed as the following two linear lines:

$$F_x = \beta_x u_x \quad (u_x < u_{x1}), \tag{10}$$

$$F_x = K_x(u_x - u_{x1}) + \beta_x u_{x1} \quad (u_x \geq u_{x1}), \tag{11}$$

where β_x is the tangential directional spring constant of the conical feeler.

Second, the relationship between the horizontal line force at bending point f_{x1} and the vertical line force, f_z, is shown in Figure 5. As is evident from this figure, f_{x1} versus f_z is almost linear in the region covering $f_x = 10$ mN/mm. In the present paper, we assume the obtained relationship approximates a solid linear line in Figure 5. If we denote horizontal force corresponding to u_{x1} as F_{x1}, F_{x1} is expressed as following equation:

$$F_{x1} = \alpha_x F_z + \gamma_x, \tag{12}$$

where α_x and γ_x are constants identified from F_z versus F_{x1}.

If we summarize Eqs. (10) to (12) and obtain expressions corresponding to Eqs. (8) and (9), assuming that the same expressions hold for the y-direction, we obtain the following expressions:

$$F_x = \begin{cases} \beta_x u_x & (u_x < u_{x1}) \\ K_x u_x + (1 - K_x/\beta_x)(\alpha_x F_x + \gamma_x) & (u_x \geq u_{x1}) \end{cases}, \tag{13}$$

$$F_y = \begin{cases} \beta_y u_y & (u_y < u_{y1}) \\ K_y u_y + (1 - K_y/\beta_y)(\alpha_y F_y + \gamma_y) & (u_y \geq u_{y1}) \end{cases}. \tag{14}$$

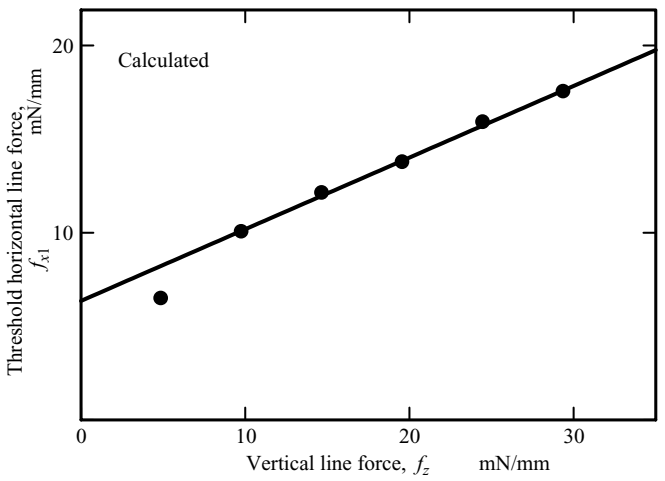

Fig. 5. Relationship between threshold of horizontal line force and vertical line force.

IV. EXPERIMENTAL APPARATUS AND EXPERIMENTAL CONDITIONS

IV.1. Rubber sheet manufacturing

The rubber sheet that incorporates these conical feelers was produced from a mold featuring an array of concave cones. The mold is shown in Figure 6. These concave cones were formed by a precise electric-discharge milling machine (MG-ED07-200, Matsushita Electric Industrial Co., LTD.). Since precision of the tactile sensor depends on the shape of the concave cones, optimal working conditions were obtained to produce the concave cones in the previous paper.[12] The mold has an array of concave cones of which the depth and base radius are 100 and 150 μm, respectively. The pitch between two concave cones and the array size were 600 μm and 10×12, respectively. After the silicon rubber sheet was produced by pouring viscous fluid silicon rubber (KE-1404, Shin-Estu Silicon) into the mold, Molds A and B were assembled as shown in Figure 6. The viscous fluid silicon rubber hardened by a catalyst that was added to the viscous fluid silicon. After that, it was cured for almost 1 day at room temperature and for 1 hour at 120°C to reduce changes with passage of time.

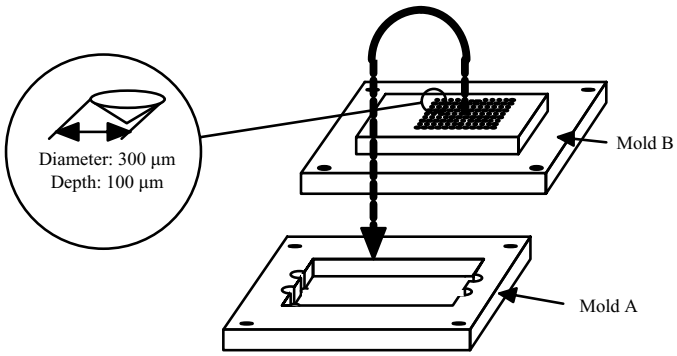

Fig. 6. Molds for the rubber sheet.

https://doi.org/10.1017/S0263574704001535 Published online by Cambridge University Press

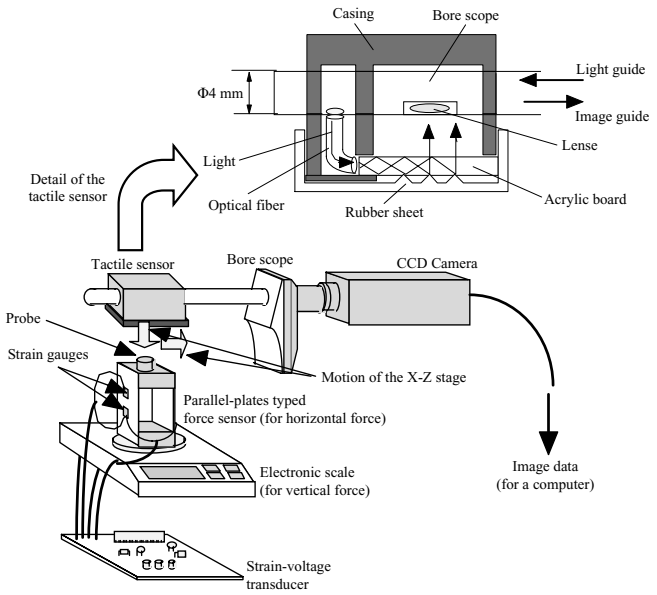

Fig. 7. A micro three-axis tactile sensor system.

IV.2. Micro three-axis tactile sensor system

An experimental tactile sensing system comprised the abovementioned silicon rubber sheet, an acrylic board, a micro-bore scope (C040-032-090-50, Olympus Co.), a Xenon light source (1LV-2, Olympus Co.), a monochrome chilled CCD camera (C5985, Hamamatsu Photonics), a frame memory board (CT-9800B, Cyber Tech, Co.), and a computer (PC-9801RA, NEC), as shown in Figure 7. The bore scope is a type of microscope used for internal observation of a straight tubule. Light emitted from a light source in the bore scope is introduced into one side of the acrylic board, functioning as an optical waveguide. Distributed light spots caused by contact with conical feelers on the rubber sheet and the acrylic board are detected by the CCD camera through the bore scope and are accumulated into the frame memory board built into the computer. The normal force applied to the sensing surface of the tactile sensor is measured by an electric scale (resolution: 0.1 mN) and is sent to the computer through an RS232C interface. The shearing force is measured by a load cell created through our own work. The load cell consists of a pair of parallel flat springs with four strain gauges plastered to their surfaces and was calibrated with the electric scale. Output signals from the strain gauges are transferred to the computer through a strain amplifier and an A/D converter board. The total resolution for sensing shearing force is about 0.1 mN. The tactile sensor, the bore scope and the CCD camera are equipped with a precision X-Z stage. Two-dimensional force is applied to the sensing surface of the tactile sensor with the adjustment of a precision feed screw of the X-Z stage.

IV.3. Experimental conditions

In order to validate the sensing principle of the present tactile sensor, we performed a series of experiments using the abovementioned tactile sensing system. After adjusting the position of the sensing surface to make the contact area of a probe mounted on the end of the parallel-plate-type force sensor cover the 3×3 conical feelers, a two-dimensional force was applied to the sensing surface. In experiments for detecting the normal force, only a normal force is applied to the feelers with stepwise increase in force. Upon each increase in force, the contact area of a conical feeler centering in an image is processed, and the gray-scale values of the image data are integrated within a sub-window of 460 μm × 460 μm, centering at the conical feeler's tip position. On the other hand, after applying an initial normal force $F_z = 2.2, 4.4, 6.5, 8.7, 10.9$ mN to the sensing surface, F_x is increased in a stepwise manner from 0 to 10 mN. Then, upon each increase in force, the centroid of the gray-scale values within the sub-window is calculated, as is the integration of gray-scale values.

V. EXPERIMENTAL RESULTS AND DISCUSSION

V.1. Normal force detection test

To validate normal force detection, after starting from the initial load of 0 mN, the normal force is increased in a stepwise manner. When the applied force reaches the maximum force, the normal force decreases in a stepwise fashion until it returns to 0 mN. Figure 8 shows the relationship between the integrated gray-scale value and the applied normal force. Since the applied force through the probe transmits to nine contact feelers as mentioned above, the value of the applied normal force is divided by nine to obtain the characteristic of a conical feeler. Values of the ordinate and abscissa of Figure 8 are converted to values for a conical feeler.

As is evident from Figure 8, the relationship is almost linear in the low-applied force region below 12 mN. However, the slope of the relationship increases abruptly in the high-applied force region over 12 mN. This is because the contact area increases rapidly due to new contact areas between the two adjacent conical feelers. The hysteresis loop observed in the high-applied force region is not observed in the low-applied force region, indicating that our sensor functions

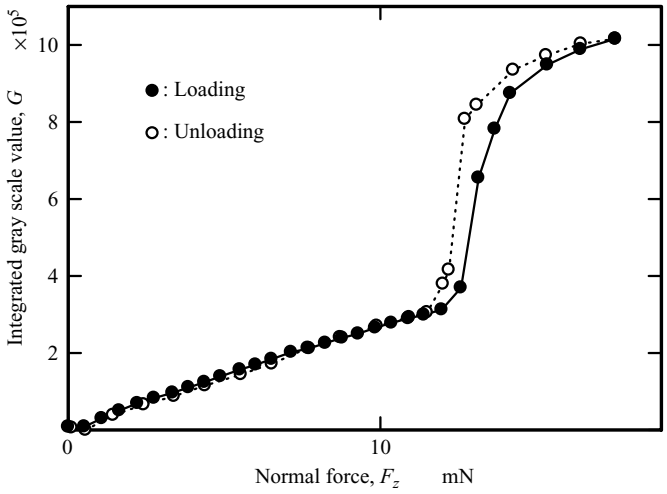

Fig. 8. Relationship between integrated gray scale value and normal force.

https://doi.org/10.1017/S0263574704001535 Published online by Cambridge University Press

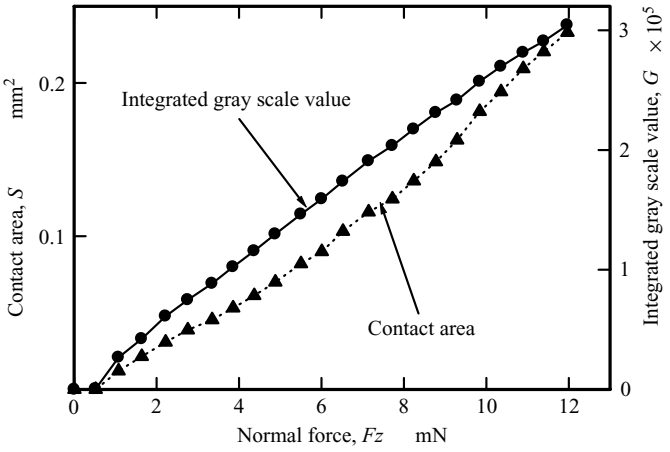

Fig. 9. Comparison between contact area and integrated gray-scale value for estimation of normal force.

as a precise load cell in the region from 0 to 12 mN for each conical feeler.

In the previous study, we adopted contact areas to obtain values of applied normal force. The relationship between contact area and applied normal force is shown in Figure 9 in order to compare the ordinal method with the present gray-scale integral method. Additionally, the aforementioned relationship of $G - F_z$ is superimposed on Figure 9. As is evident from this figure, the present gray-scale integral method is superior to the ordinal contact area method at the point of linearity.

V.2. Relationship between gray-scale value and contact pressure

To examine why the present gray-scale integral method is superior to the ordinal contact area method at the point of linearity, we consider relationship between the gray-scale value and contact pressure. The distribution of the gray-scale value of contact image is obtained from the previous normal-force loading test. Figure 10(a) shows the distributed gray-scale value at the contact area's center. However, because we cannot measure contact pressure, we use a simulated contact pressure calculated by the 3-D model as shown in Fig 10(b). Both of these figures show bell-shaped distribution. Using results of Figures. 10(a) and (b), we obtain the relationship between contact pressure and gray-scale value and show it in Figure 11. As is evident from Figure 11, the relationship between contact force p and gray-scale value g shows good linearity.

On the other hand, it has been derived from theoretical analysis performed on a Gaussian distributed surface unevenness that the real contact area is proportional to the contact pressure.[13] Since fine unevenness resulting from the electric-discharge milling exists on the surface of the conical concave of the mold, each conical feeler's surface includes fine unevenness due to transcription. Furthermore, because the real contact area is obtained from the sum effect of numerous tiny contact areas on the small convex tips produced by the contact of the fine uneven surface and the acrylic flat surface, the real contact area seems to be proportional to the gray-scale value. Therefore, the present

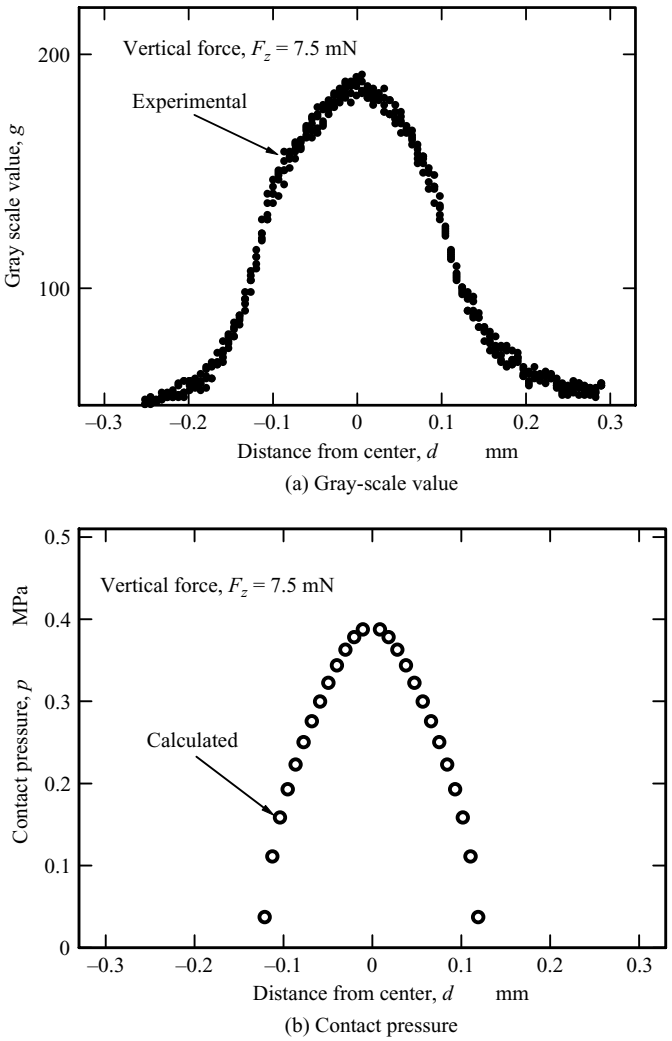

Fig. 10. Spatial distribution of gray-scale value and contact pressure (a) Gray-scale value (b) Contact pressure.

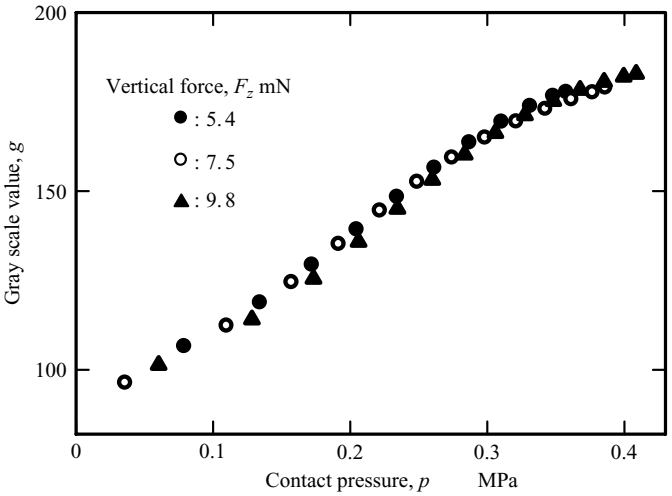

Fig. 11. Relationship between contact pressure and gray-scale value.

experimental result verifies the abovementioned theoretical analysis.

Linearity between contact area and applied force does not hold in the case of the imperfect conical feeler used

https://doi.org/10.1017/S0263574704001535 Published online by Cambridge University Press

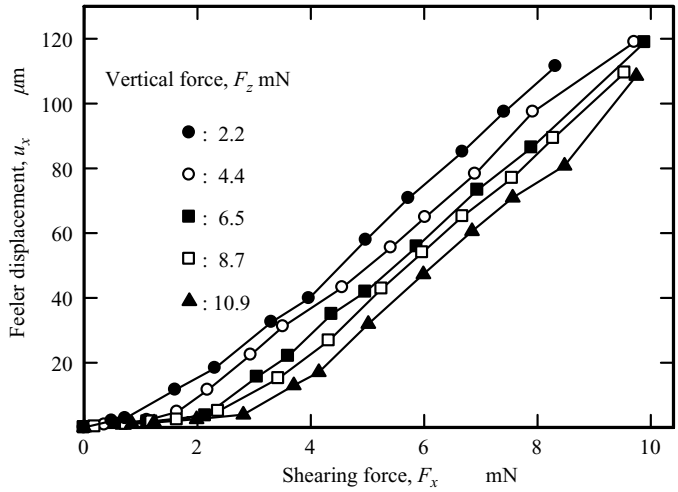

Fig. 12. Relationship between horizontal displacement of the conical feeler and shearing force.

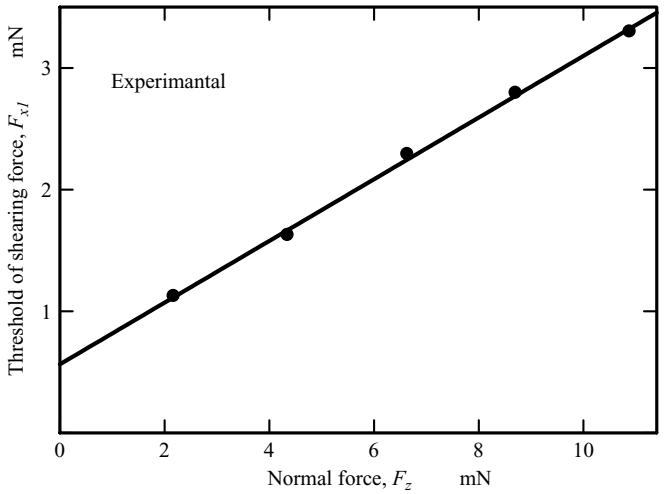

Fig. 13. Dependence of normal force on slippage initiation caused by shearing force.

in the present study. As is evident from the aforementioned discussion, the estimation method using the gray-scale value can be applied to a wider measuring range that maintains high linearity. Particularly, in addition to the difficulty of making a perfectly conical shape for smaller feelers, the influence of surface unevenness on the feelers' dimensions increases. Therefore, the present gray-scale method is effective for the micro-tactile sensor.

V.3. Combined loading test of normal and shearing force

In order to evaluate Eqs. (10) to (12), after applying the initial normal force of $F_z = 2.2, 4.4, 6.5, 8.7, 10.9$ mN onto the sensing surface, F_x was increased in a stepwise manner from 0 to 10 mN while maintaining a constant normal force. Upon each increase in force, the centroid of gray-scale values within the aforementioned sub-window was calculated and the displacement of the centroid from the initial position was called u_x. In Figure 12, the ordinate and abscissa represent the horizontal force, F_x, and the centroid displacement, u_x, respectively.

As is evident from Figure 12, the low- and high-load regions exhibit different sensitivity coefficients. This is a similar inclination to the simulated results discussed in Section 3.2. Also clear is that the inflection point F_{x1} moves horizontally as the normal force increases. Moreover, slopes of u_x in the region exceeding F_{x1} are almost constant, even if F_z is varied. Furthermore, from the high-load region, the spring constant K_x included in Eq. (11) is estimated to obtain $K_x = 0.067$ mN/μm. Additionally, from the low-load region, the sensitivity to a low load, β_x is estimated to obtain $\beta_x = 1.7$ mN/μm.

Next, for each initial normal force condition, the relationships between u_x and F_x are approximated to bi-linear lines, and the shearing force causing slippage, F_{x1}, is calculated from the intersection of the bi-linear lines. As is evident from Figure 13, which shows the variation in F_{x1}, F_{x1} is almost proportional to F_z. If α_x and β_x included in Eq. (12) are estimated from Figure 13, we obtain $\alpha_x = 0.25$ and $\gamma_x = 0.56$ mN.

Finally, we show variation in G under a stepwise increase of F_x and constant F_z in Figure 14 to determine whether the relationship between G and F_z is not influenced by a variation in F_x. In fact, Figure 14 indicates that G maintains a constant value even if F_x increases. Figure 15 shows a comparison between relationships of $G - F_z$ with shearing force and without shearing force. In Figure 15 the solid circles represent the relationship with the shearing force obtained from Figure 14, and it is clear that both of the relationships almost coincide in Figure 15. Since the magnitude of the shearing force has no influence on the sensitivity characteristic in the normal direction, it is possible to identify the shearing force and normal force independently.

Consequently, $u_x - F_x$ is expressed by Eqs. (10) to (12). Regarding sensitivities of the low- and high-load regions β_x and K_x, β_x is 25 times higher than K_x. This result suggests that the present tactile sensor can function as a high-sensitivity sensor in the low-load region.

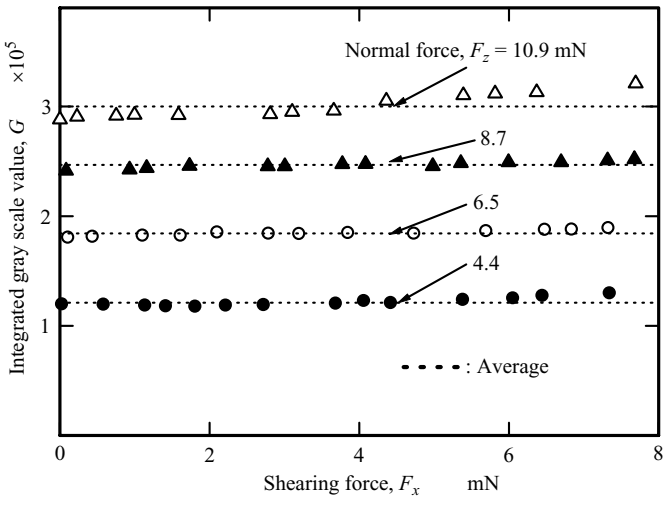

Fig. 14. Variation in integrated gray-scale value under applied shearing force.

https://doi.org/10.1017/S0263574704001535 Published online by Cambridge University Press

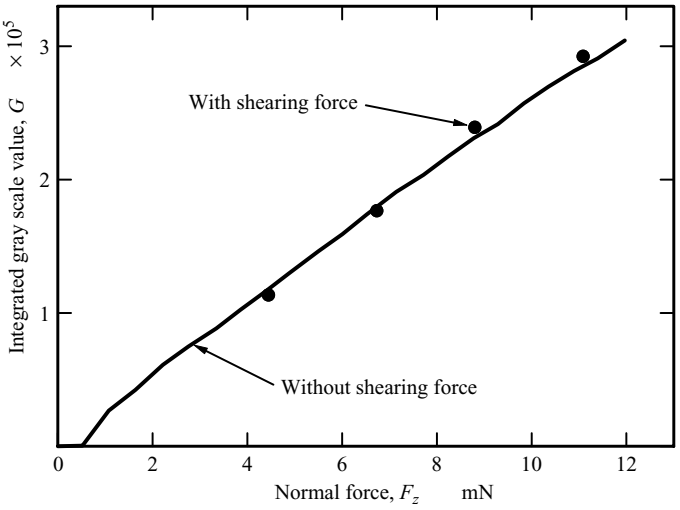

Fig. 15. Relationship between normal force and integrated gray-scale value.

VI. CONCLUSION

We proposed a principle for the three-axis tactile sensor intended for mounting on a microscope-shaped micro-robot, and confirmed the adequacy of the principle with a trial model.

When we compared the distribution of gray-scale values of contact images obtained from experiments and distributed pressure calculated from 3-D FEM contact analysis, we found that both of these distributions showed bell-shaped distributions. In addition, the relationship between contact pressure and gray-scale value showed good linearity. Because of this result, the gray-scale value of each pixel corresponds to the real contact area of small convex tips, which results from the contact of a fine uneven surface with an acrylic flat surface. Consequently, instead of the ordinal contact area method, the estimation method using gray-scale values can be applied to a wider measuring range that maintains high linearity.

Next, if we increase the shearing force under constant normal force, in the low-load region, the centroid of contact moves slightly and in the subsequent high-load region, it moves markedly. Results also revealed that the inflection point moves horizontally as the normal force increases. Moreover, variation in the inflection point is almost proportional to the vertical force.

Finally, the integrated gray-scale value remains constant, even if the normal force increases. Since the magnitude of the shearing force has no influence on the sensitivity characteristic in the vertical direction, the shearing force and the normal force can be identified independently.

Acknowledgement

This work was supported by fiscal grants from the Ministry of Education of Japan (Grant-in-Aid for Scientific Research (A), No. 07555057) and the Micro-Machine Center.

References

1. H. R. Nicholls, *Advanced Tactile Sensing for Robotics* (H. R. Nicholls, ed.) (World Scientific Publishing, Singapore, 1992) pp. 13–47.
2. D. H. Mott, M. H. Lee and H. R. Nicholls, "An Experimental Very High Resolution Tactile Sensor Array," *Proc. 4th Int. Conf. On Robot Vision and Sensory Control* (1984) pp. 241–250.
3. K. Tanie, K. Komoriya, M. Kaneko, S. Tachi and A. Fujiwara, "A High Resolution Tactile Sensor Array," *Robot Sensors Vol. 2*: *Tactile and Non-Vision* (IFS Publ., UK 1986) pp. 189–198.
4. H. R. Nicholls, "Tactile Sensing Using an Optical Transduction Method," *Traditional and Non-traditional Robot Sensors* (Edited by T. C. Henderson) (Springer-Verlag, 1990) pp. 83–99.
5. H. Maekawa, K. Tanie, K. Komoriya, M. Kaneko, C. Horiguchi and T. Sugawara, "Development of Finger-shaped Tactile Sensor and Its Evaluation by Active Touch," *Proc. of the 1992 IEEE Int. Conf. on Robotics and Automation* (1992) pp. 1327–1334.
6. S. Guo, T. Fukuda, K. Kosuge, F. Arai, K. Oguro and M. Negoro, "Micro-Catheter Micro System with Active Guide Wire," *Proc. 1995 IEEE Int. Conf. On Robotics and Automation* (1995) pp. 79–84.
7. T. Mineta, T. Mitsui, Y. Watanabe, S. Kobayashi, Y. Haga and M. Esashi, Batch Fabricated Flat Meandering Shape Memory Alloy Actuator for Active Catheter, *Sensors and Actuators* **A 88**, 112–120 (2001).
8. K. Yoshida, M. Kikuchi, J.-H. Park and S. Yokota, "Fabrication of Micro Electro-rheological Valves (ER Valves) by Micromachining and Experiments," *Sensors and Actuators*, **A 95** 227–233 (2002).
9. M. Ohka, Y. Mitsuya, S. Takeuchi, H. Ishihara and O. Kamekawa, "A Three-axis Optical Tactile Sensor (FEM Contact Analyses and Sensing Experiments Using a Large-sized Tactile Sensor)," *Proc. of the 1995 IEEE Int. Conf. on Robotics and Automation* (1995) pp. 817–824.
10. M. Ohka, Y. Mitsuya, K. Hattori and I. Higashioka, "Data Conversion Capability of Optical Tactile Sensor Featuring an Array of Pyramidal Projections," *Proc. of 1996 IEEE/SICE/RSJ Int. Conf. on Multisensor Fusion and Integration for Intelligent Systems* (1996) pp. 573–580.
11. M. Ohka, Y. Mitsuya, Y. Matsunaga and S. Takeuchi, "Sensing Characteristics of an Optical Three-axis Tactile Sensor Under Combined Loading," *Robotica* **22**, Part 2, 213–221 (2004).
12. M. Ohka, I. Higashioka and Y. Mitsuya, "A Micro Optical Three-axis Tactile Sensor (Validation of Sensing Principle Using Models)," *Advances in Information Storage Systems*, **Vol. 10** (B. Bhushan and K. Ono, eds.) (World Scientific Publishing, Singapore, 1999) pp. 313–325.
13. J. Halling, *Principles of Tribology* (The Macmillan Press, London, 1975) pp. 61–65.